Sodium ion exosphere of Mercury during MESSENGER flybys

Jan Paral,[1,2] Pavel M. Trávníček,[3,4] Robert Rankin,[1] and David Schriver[3]

Received 18 June 2010; revised 21 July 2010; accepted 3 August 2010; published 7 October 2010.

[1] Two flybys of Mercury by the NASA MESSENGER spacecraft on January 14 and October 6, 2008 provide insight into the spatial distribution of the heavy ion exosphere around the planet. The relatively quiet solar wind conditions and interplanetary magnetic field (IMF) orientation allow us to compare "in situ" observations with numerical simulations. During each flyby, the IMF had a strong radial Sun-Mercury direction but nonzero northward and southward components for the first (M1) and second (M2) flybys, respectively. We show that comparative studies of particle tracing in stationary electromagnetic fields from a self-consistent hybrid kinetic model provide a good characterization of Mercury's sodium ion exosphere when compared with MESSENGER observations. **Citation:** Paral, J., P. M. Trávníček, R. Rankin, and D. Schriver (2010), Sodium ion exosphere of Mercury during MESSENGER flybys, *Geophys. Res. Lett.*, *37*, L19102, doi:10.1029/2010GL044413.

1. Introduction

[2] An extensive study of planet Mercury began after the discovery of its intrinsic magnetic field by Mariner 10 in 1974/75 [*Ness et al.*, 1974]. It was also revealed that Mercury has an exospheric environment [*Broadfoot et al.*, 1976] not very different from Earth. Recently, the NASA MESSENGER spacecraft visited Mercury by performing three equatorial flybys on January 14, 2008 (M1), October 6, 2008 (M2), and September 29, 2009. These predate the orbital phase of the mission, which is scheduled to begin on March 18, 2011. During M1 and M2, the interplanetary magnetic field (IMF) had a strong radial Sun-Mercury component with nonzero northward component B_z during M1, and south-pointing B_z during M2. The solar wind conditions were relatively quiet for both flybys, providing two typical but quantitatively different cases of IMF orientation to investigate. From the information already provided by MESSENGER, it has been found that the intrinsic magnetic field of the planet is dipole-like, with a magnetic moment of 250 nT R_M^3 [*Slavin et al.*, 2009]. Because of sun shadowing of the spacecraft, there are no direct measurements of solar wind parameters, and estimates must come from solar wind expansion models. Nevertheless, the flybys have revealed that Mercury's magnetosphere has a striking resemblance to Earth, with similar phenomena such as Kelvin-Helmholtz vortexes on the flanks, plasmoid formation, and other phenomena [*Slavin et al.*, 2008, 2010].

[3] The MESSENGER spacecraft carries instruments relevant to the study of the heavy ion exosphere of Mercury, including Fast Imaging Plasma Spectrometer (FIPS) as a part of the Energetic Particle and Plasma Spectrometer (EPPS). The FIPS-EPPS instrument counts heavy ions for various ranges of m/q ratio, where m and q are particle mass and charge, respectively. The FIPS covers an energy range from tens of eV to 13.5 keV, and provides coverage of approximately 1.4π steradians solid angle. The actual field of view is limited by the fact that the instrument is shielded from the Sun and so caution is necessary when the sunshade is between the instrument's field of view and the bulk plasma flow direction, because only the supra-thermal population of plasma contributes to the measurement. A summary of measurements taken during the M1 flyby is given by *Zurbuchen et al.* [2008], who concluded that the most abundant heavy ion species is sodium. Although note that instrument can not differentiate between atomic masses 23 and 24. During the M1 flyby FIPS recorded an accumulation of Na^+ on the dusk side in the equatorial plane and in the vicinity of the inbound magnetopause crossing. Note that data from M2 were not published as of this writing.

[4] The source of Mercury's sodium exosphere is the surface of the planet, which refills the planetary environment by ejecta from the regolith. At least two major releasing processes contribute to the source of this new material: Photon-Stimulated Desorption (PSD) and Solar Wind Sputtering (SWS). The PSD process is active on the dayside of the planet, with the maximum flux of ejected particles occurring at the sub-solar point because of solar wind photons that directly excite surface atoms. The SWS process is due to solar wind ions and energetic atoms that impinge on the surface at highly localized auroral and mid-latitude regions, as discussed by *Paral et al.* [2009].

[5] The objective of this paper is to carry out quantitative numerical studies of two cases that are similar to the M1 and M2 flybys. We model the spatial distribution of the sodium ion exosphere, and compare it with data taken by MESSENGER during the first flyby. The methodology involves test-particle ion tracing in the electromagnetic fields provided by a self-consistent hybrid model. This extends previous work by *Sarantos et al.* [2009].

2. Initialization

2.1. Hybrid Simulation

[6] In our studies, we use the hybrid self-consistent numerical model, where ions are treated kinetically and electrons are described as a massless charge neutralizing fluid. The system consists of a 3D rectangular cartesian grid

[1]Department of Physics, University of Alberta, Edmonton, Alberta, Canada.
[2]Department of Space Physics, Institute of Atmospheric Physics, Academy of Sciences of the Czech Republic, Prague, Czech Republic.
[3]Institute of Geophysics and Planetary Physics, University of California, Los Angeles, California, USA.
[4]Astronomical Institute, Academy of Sciences of the Czech Republic, Prague, Czech Republic.

0094-8276/10/2010GL044413

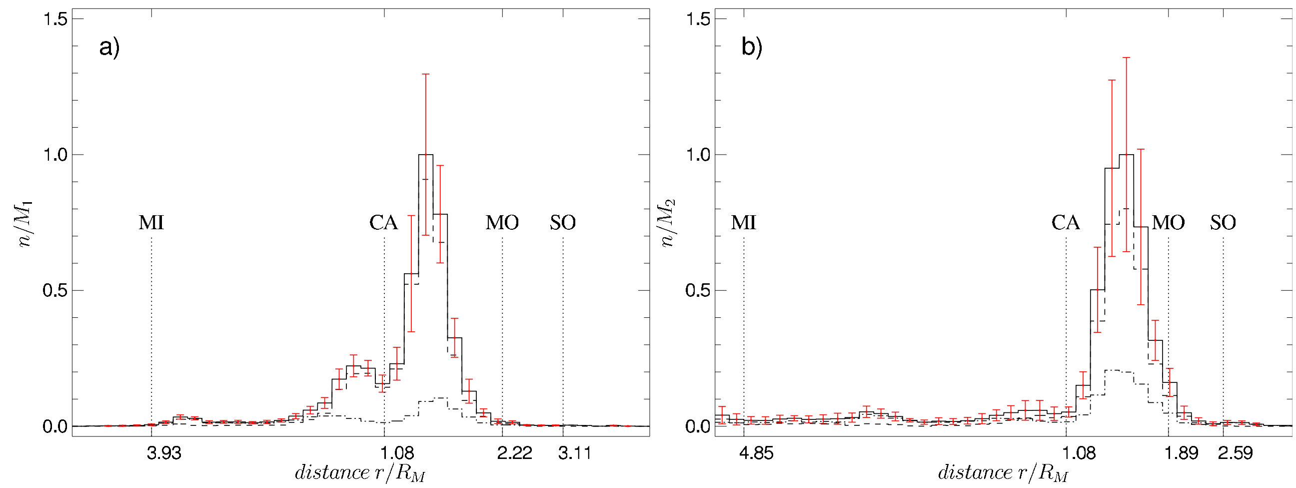

Figure 1. Measurements of sodium ion density in arbitrary units of virtual flyby using the trajectory from the (a) first and (b) second flyby of MESSENGER, respectively. Ejecting mechanisms PSD and SWS are represented by dashed and dashed-dotted lines, respectively, and the sum of both is represented by the solid line. Locations of magnetopause inbound, closest approach and magnetopause outbound are marked as MI, CA and MO, respectively. Scaling factors $M_{1,2}$ = 13.7 and 4.7 ions/cc for the first and second flyby, respectively.

with spatial resolution $dL = 0.4 \times 1.0 \times 1.0c/\omega_{p,sw}$, where c is the speed of light and $\omega_{p,sw}$ is the solar wind proton plasma frequency. The simulation box domain length is $L = 237.6 \times 286 \times 286c/\omega_{p,sw}$. We use background fields obtained from two simulations described in detail by *Trávníček et al.* [2007]. The IMF is defined through its Cartesian components with northward $\mathbf{B}^{IMF} = (0.94, 0, 0.34)B_{sw}$ and southward IMF $(0.94, 0, -0.34)B_{sw}$ corresponding to HYB1 and HYB2, respectively. We assume solar wind parameters: magnitude of IMF B_{sw} = 18 nT; solar wind density of protons n_{sw} = 32 cm^{-3} for both study cases.

2.2. Particle Tracing

[7] We consider photo-stimulated desorption (PSD) and solar wind sputtering (SWS) to be two major release mechanisms responsible for refilling the exosphere of Mercury with neutral and ionized sodium. Each process releases particles as neutral atoms but 1% of sodium is already ionized when ejected [*Milillo et al.*, 2005]. We neglect micro-meteorite vaporization because the contribution to the total content of exospheric sodium is not expected to exceed ~20% and ~4% of SWS and PSD, respectively [*Killen et al.*, 2004].

[8] The spatial distribution of solar wind sputtering is highly dependent on the orientation of the IMF [*Delcourt et al.*, 2003]. The orientation and magnitude of the IMF is also a key parameter responsible for opening the magnetosphere to entry of solar wind ions along open field lines. The energy transmitted during each sputtering interaction is $T = T_m \cos^2(\alpha_r)$, where α_r is the recoil angle and the maximal transmitted energy T_m between an incident particle with energy E_i and mass m_1, and sputtered particle of mass m_2, is given by $T_m = E_i(4m_1m_2)/(m_1 + m_2)^2$. We only consider H^+ and Na/Na^+ to be the interacting species. The energy distribution function is described by

$$f_s(E_e, T_m) = \frac{E_e}{(E_e + E_b)^3}\left[1 - \left(\frac{E_e + E_b}{T_m}\right)^{1/2}\right] \quad (1)$$

where E_b = 2 eV is the surface binding energy, E_e is the energy of the emitted particle. We consider T_m to be 500 eV in both cases. The angular distribution function is $\cos^\gamma(\alpha_n)$, where γ is a number between 1 and 2 (in our case, we use 1) and α_n is the angle between the normal to the surface and the initial velocity. The total number of particles ejected from the surface per second Φ^{SWS} was estimated by *Killen et al.* [2004] to be between 6.0×10^{21} and 3.8×10^{24} s^{-1} particles, based on solar wind parameters that range from n_{sw} = 10–90 cm^{-1}, v_{sw} = 350–750 km s^{-1}, and 5–30% of the surface open to the solar wind. Assuming the solar wind conditions to be n_{sw} = 32 cm^{-1}, v_{sw} = 350 km s^{-1}, and surface open to the solar wind to be 17.0% and 13.7%, respectively, we set the flux Φ_0^{SWS} to be 9.6×10^{23} and 8.0×10^{23} s^{-1} for HYB1 and HYB2, respectively. We apply a self-consistent flux distribution of solar wind protons over the planet surface using results of the hybrid simulations of *Trávníček et al.* [2007] as initial conditions for our model, as well as in determining the surface area which is open to solar wind protons.

[9] The energy distribution function of photon-stimulated desorption can be closely approximated [*Johnson et al.*, 2002] by the energy distribution function:

$$f(E) = x(1 + x)\frac{EU^x}{(E + U)^{2+x}} \quad (2)$$

where x = 0.7 and U = 0.052 eV. This function has its maximum at approximately half of the binding energy U, and contains a long high energy tail as compared to the Maxwell-Boltzmann energy distribution [*Mura et al.*, 2007]. The surface flux of ejected particles is dependent on the angle ϕ between zenith and the subsolar point and is defined as $\Phi_n(\phi) = \Phi_n{}^* \cos(\phi)(R/R^*)^2$.

[10] The number of particles through the surface Φ^{PSD} is unknown but was estimated by *Killen et al.* [2004] to be between 5.0×10^{24} and 1.0×10^{25} s^{-1}. We choose a PSD rate of $\Phi_0^{PSD} = 5.0 \times 10^{24}$ s^{-1} for both simulations as it provides a baseline fit to the MESSENGER UV measure-

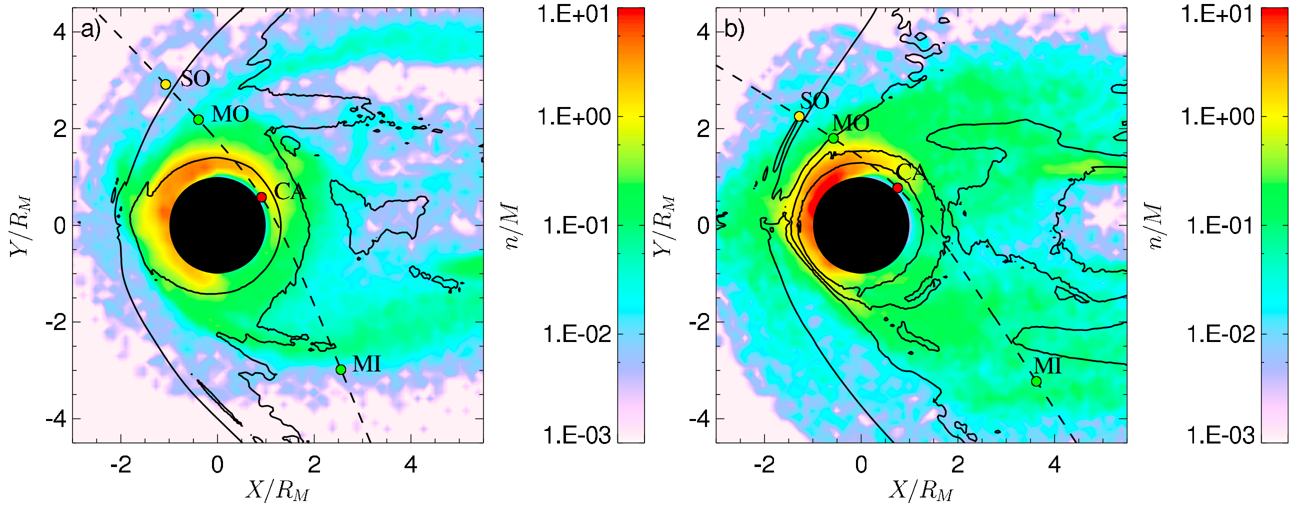

Figure 2. Color representation of sodium ion (Na^+) density in equatorial plane (X, Y). (a and b) Solar wind conditions which we refer to as HYB1 and HYB2, respectively. Dashed line represents projection of trajectory of M1 and M2 flybys of MESSENGER on equatorial plane, respectively. Colored markers show position of magnetopause inbound (MI), closest approach (CA), magnetopause outbound (MO) and shock outbound (SO) crossings as determined from hybrid simulations. The iso-contours represent constant magnetic field $|B|$ of 1.6 and 5 B_{sw}.

ments of emission from neutral Na [*Burger et al.*, 2010]. Note, however, the PSD flux must be increased by a factor of 4 on areas open to the solar wind to match the sodium enhancements observed by MESSENGER above Mercury's polar regions.

[11] Peak ion densities in Figures 1a and 1b along the virtual trajectory are normalized by the factor $M_{1,2}$ = max $(n_{SWS} + n_{PSD})$ where $M_1 = 13.7$ and $M_2 = 4.7$ ions cm^{-3} for HYB1 and HYB2, respectively. The factors M_1 and M_2 correspond to the values of Φ_0^{PSD} and Φ_0^{SWS} defined earlier, assuming the density scales linearly with the surface flux.

[12] The photoionization life time τ_p for sodium was estimated to be $5 \times 10^4 - 4 \times 10^5$ s at a mean orbit of 0.386 AU [*Milillo et al.*, 2005]. Because photoionization is dependent on photon flux, we scale the ionization time using the actual distance from the Sun during the given flyby using $\tau = \tau^*(R/R^*)^2$ where $R^* = 0.386$ AU and R is the distance from the Sun (0.307–0.467 AU). We use values of 0.353 and 0.341 AU for M1 and M2, respectively. For both simulations we use $\tau_p^* = 5 \times 10^4$ s. Each neutral particle carries a weight w of unity at the time of surface ejection. This value is decreased every time step by $dw/dt = w(t)\tau_p^{-1}$, where τ_p is a typical photoionization time. We neglect ionization due to charge exchange which has a much longer ionization time. The weight decrement dw is accumulated on the mesh and when it reaches unity an ion is released in the given cell with the local velocity distribution of the neutral particles. In the neutral state, only gravitation and acceleration pressure forces act on particles. The gravity force is approximately 3.697 m/s^2 but the radiation pressure acceleration a_{rp} varies due to the Doppler shifted photon flux, and can be between 0.2 and 2 m/s^2. To account for the relative velocity of the planet and Sun during the flybys we assume a_{rp} to be ~1.8 m/s^2 for both simulations.

3. Results

[13] The spatial distribution of neutral atoms is governed by gravitation and radiation pressure forces as well as the energy distribution and spatial distribution of releasing processes. In the case of SWS the energy of neutral particle ejecta is high enough to easily escape bounding forces and forms a corona-like envelope. On the other hand, the PSD process releases relatively low energy particles with energy distribution peak at 0.1 eV [*Yakshinskiy and Madey*, 1999]. These particles are bound by gravitational force to the planetary surface and form a thin layer with a maximal altitude of ≈80 km at the nose of the planet. This layer is a rich source of ions because of the increased chance of photoionization. Ionized particles are governed only by electromagnetic fields and so the orientation of the IMF plays a dominant role in determining the ion distribution.

[14] Figure 2 presents the spatial distribution of sodium ions (Na^+) in the equatorial plane. Figures 2a and 2b represent HYB1 and HYB2 simulation results respectively, with MESSENGER trajectories from the first and second flybys represented by a dashed line. The color markers MI, CA, MO and SO represent magnetopause inbound, closest approach, magnetopause outbound and shock outbound, respectively (as observed from the hybrid simulation). The color scale represents sodium ion density scaled in arbitrary units defined above. The axes are scaled to the radius of Mercury R_M with the Sun in the −X direction. The solid line contours represent constant magnitude of the magnetic field of 1.6 B_{sw} and 5 B_{sw} for easy identification of magnetosphere structure.

[15] As a result of the different orientation of the IMF, sodium distribution in the equatorial plane in Figure 2 differs between HYB1 and HYB2. Particles easily leak upstream at the subsolar point in the case of south-pointing IMF as seen Figure 2b. The prominent feature of northward pointing IMF in Figure 2a corresponds to an accumulation of sodium ions in the downstream predawn magnetosphere sector. This is in agreement with observations from the FIPS during the first flyby. Particles near closest approach have average energy per bin of 3 keV. On the other hand, a high energy ion population, with average energy 10 keV, can be observed upstream of the magnetopause. This distribution of energetic ions is different for HYB1 and HYB2; for north

pointing IMF (i.e. HYB1) energetic particles are accumulated at the dawn flank whereas for south pointing IMF they are present from the dayside to post-dusk sector.

[16] In general, ionized particles are carried westward and are transported to the night-side where they can escape into the tail or back-scatter on the surface. Note the differences for both cases of IMF in Figure 2. For northward B_z we can clearly see that the ion population is confined downstream of the magnetopause. On the other hand, southward pointing IMF allows particles to escape at the nose of the magnetosphere due to reconnection.

[17] Ions released by SWS are originally localized at auroral mid-latitude regions. The velocity distribution points in the direction normal to the surface and thus the parallel velocity with respect to the local magnetic field is greater than the perpendicular velocity. Such particles are partially trapped and undergo mirror motion with a relatively high latitude mirror point. The remaining particles escape and are lost to the tail where they follow a meandering motion.

[18] In the case of PSD, particles have rather small energy after being released and form a thin layer of neutral particles on the dayside which acts as a source of photo-ions. Ionized particles have small parallel velocity as compared to their perpendicular velocity and thus PSD ions equatorially mirror before back-scattering to the surface. Because of the different removal mechanism, PSD is responsible for filling lower altitudes with low energy particles. SWS, on the other hand, is most likely filling the higher altitude regions.

[19] Figure 1 represent virtual flybys through simulated data. Figures 1a and 1b represent the two study cases HYB1 and HYB2 that correspond approximately to the solar wind conditions appropriate to M1 and M2 flybys of MESSENGER, respectively. The error bars represent one standard deviation of simulated data using a sequence of time slices of EM fields taken from hybrid model. The fields are taken exactly one gyroperiod apart. The large error bars in Figure 1 reveal the importance of wave-particle interactions in determining the observed sodium density. As expected, the high density region near the closest approach is more susceptible to plasma dynamics. In the near Mercury environment, magnetically trapped particles undergo bouncing motion between conjugate hemispheres while interacting with low frequency waves. These waves have frequency close to the proton gyrofrequency and affect the topology of electromagnetic fields which in turn change the local distribution of sodium ions.

[20] Direct measurements of M1 [*Zurbuchen et al.*, 2008] reveal several ion density accumulation regions along the flyby trajectory that qualitatively agree with our models: First, increased density in the inbound leg when crossing the magnetopause; second, a gradual increase of density as the spacecraft approaches the planet, followed by a sudden decrease before crossing the CA. This decrease is due to the large particle gyroradius, which diffuses particles to higher L-shell as they drift into the night sector. Diffusion is likely responsible for density depletion near the noon sector of the planet, as seen in the vicinity of closest approach in the FIPS measurements as well as our virtual flyby.

4. Conclusions

[21] Simulations reveal that in the near Mercury environment, photon stimulated desorption (PSD) is the dominant source of the exosphere (compare Figure 1). This results from a relatively high density source of low energy neutral particles on the dayside, although we note that thermal desorption that is difficult to quantify with our model may reduce the PSD process.

[22] Photoionization on the dayside acts as a fountain which replenishes the exosphere with new Na^+ ions. On the other hand, SWS ejects particles from a narrow band of high latitudes in the auroral region that fill the tail of Mercury with new Na^+.

[23] By comparing numerical results with data from the MESSENGER FIPS published by *Zurbuchen et al.* [2008], we conclude that our numerical studies are in good agreement compared to M1, where a comparison can be made. Density accumulation occurs downstream of the dusk magnetopause, with maximum density occurring after closest approach as MESSENGER moves outbound toward the magnetopause, which is located in the dawn sector of the equatorial plane. Peak ion densities along the MESSENGER orbit correspond to ~14 and 5 ions cm^{-3} in our model for the first and second flyby, respectively, if the rate of 5×10^{24} Na neutrals s^{-1} is assumed for PSD. The model then predicts ~0.3 and 0.8 cm^{-3} ion densities at the outbound magnetopause for HYB1 and HYB2, respectively. Such high ion densities may explain the boundary layer feature that corresponds to the diamagnetic decrease of the magnetic field observed by *Slavin et al.* [2008, 2009] during MESSENGER flybys. The dynamic nature of our simulations reveals that plasma within 1.3 R_M radius is affected by wave-particle interactions. This region ranges from the predawn to postnoon sector.

[24] Several factors potentially contribute to differences between the observations of *Zurbuchen et al.* [2008] and our results: First, because the resolution of the "in situ" data measurements is somehow small due to the selected bin size, it is difficult to localize the peaks and valleys. Second, several species are included with rather large m/q range as compared to our results, where we include only sodium ions. Third, limitations of the FIPS sensor caused by instrument orientation, and the fact that it is on the sun shaded side of the spacecraft. Also, we include a full spectrum of ion energies, whereas FIPS is limited by its energy range sensitivity. The energy sensitivity will play an important role in the regions where low energy ions dominate such as downstream of the magnetopause on the portion of the outbound leg.

[25] **Acknowledgments.** The authors acknowledge the support by NASA MESSENGER grant NNX09AD41G, NASA MESSENGER Participating Scientist grant NNX07AR62G, and financial support from CSA and NSERC.

References

Broadfoot, A. L., D. E. Shemansky, and S. Kumar (1976), Mariner 10: Mercury atmosphere, *Geophys. Res. Lett.*, *3*, 577–580.

Burger, M. H., et al. (2010), Monte Carlo modeling of sodium in Mercury's exosphere during the first two MESSENGER flybys, *Icarus*, *209*, 63–74, doi:10.1016/j.icarus.2010.05.007.

Delcourt, D. C., et al. (2003), A quantitative model of the planetary Na^+ contribution to Mercury's magnetosphere, *Ann. Geophys.*, *21*, 1723–1736.

Johnson, R. E., F. Leblanc, B. V. Yakshinskiy, and T. E. Madey (2002), Energy distributions for desorption of sodium and potassium from ice: The Na/K ratio at Europa, *Icarus*, *156*, 136–142, doi:10.1006/icar.2001.6763.

Killen, R. M., M. Sarantos, A. E. Potter, and P. Reiff (2004), Source rates and ion recycling rates for Na and K in Mercury's atmosphere, *Icarus*, *171*, 1–19, doi:10.1016/j.icarus.2004.04.007.
Milillo, A., et al. (2005), Surface-exosphere-magnetosphere system of Mercury, *Space Sci. Rev.*, *117*, 397–443, doi:10.1007/s11214-005-3593-z.
Mura, A., A. Milillo, S. Orsini, and S. Massetti (2007), Numerical and analytical model of Mercury's exosphere: Dependence on surface and external conditions, *Planet. Space Sci.*, *55*, 1569–1583, doi:10.1016/j.pss.2006.11.028.
Ness, N. F., K. W. Behannon, R. P. Lepping, Y. C. Whang, and K. H. Schatten (1974), Magnetic feld observations near Mercury: Preliminary results from Mariner 10, *Science*, *185*, 151–160.
Paral, J., P. M. Trávníček, K. Kabin, R. Rankin, and T. H. Zurbuchen (2009), Spatial distribution and energy spectrum of heavy ions in the Hermean magnetosphere with applications to MESSENGER flybys, *Adv. Geosci.*, *15*, 1–16.
Sarantos, M., et al. (2009), Sodium-ion pickup observed above the magnetopause during MESSENGER's first Mercury flyby: Constraints on neutral exospheric models, *Geophys. Res. Lett.*, *36*, L04106, doi:10.1029/2008GL036207.
Slavin, J. A., et al. (2008), Mercury's magnetosphere after MESSENGER's first flyby, *Science*, *321*, 85–89, doi:10.1126/science.1159040.
Slavin, J. A., et al. (2009), MESSENGER observations of Mercury's magnetosphere during northward IMF, *Geophys. Res. Lett.*, *36*, L02101, doi:10.1029/2008GL036158.
Slavin, J. A., et al. (2010), MESSENGER observations of large flux transfer events at Mercury, *Geophys. Res. Lett.*, *37*, L02105, doi:10.1029/2009GL041485.
Trávníček, P. M., P. Hellinger, and D. Schriver (2007), Structure of Mercury's magnetosphere for different pressure of the solar wind: Three dimensional hybrid simulations, *Geophys. Res. Lett.*, *34*, L05104, doi:10.1029/2006GL028518.
Yakshinskiy, B. V., and T. E. Madey (1999), Photon-stimulated desorption as a substantial source of sodium in the lunar atmosphere, *Nature*, *400*, 642–644, doi:10.1038/23204.
Zurbuchen, T. H., et al. (2008), MESSENGER observations of the composition of Mercury's ionized exosphere and plasma environment, *Science*, *321*(5885), 90–92, doi:10.1126/science.1159314.

J. Paral and R. Rankin, Department of Physics, University of Alberta, 11322-89 Ave., Edmonton, AB T6G 2G7, Canada. (jparal@phys.ualberta.ca)

D. Schriver and P. M. Trávníček, Institute of Geophysics and Planetary Physics, University of California, Slichter Hall 90095-1567, Los Angeles, CA 90095, USA.